# Measuring Short-Range Correlations with ALERT

J. Barrow, A. Denniston, L. Ehinger, J. Estee, O. Hen (co-spokesperson),
J. Kahlbow, I. Korover, T. Kutz, J. Phelan, J. Pybus, H. Qi, N. Wright
Massachusetts Institute of Technology, Cambridge, MA

B. Briscoe, S. Ratliff, A. Schmidt (co-spokesperson), E. Seroka
George Washington University, Washington DC

C. Fogler, M. Hattawy, L.B. Weinstein (co-spokesperson)
Old Dominion University, Norfolk, VA

E. Piasetzky (co-spokesperson),
Tel-Aviv University, Tel Aviv, Israel

F. Hauenstein (contact person), D. Higinbotham, D.
Nguyen, S. Stepanyan, H. Szumila-Vance, X. Wei
Thomas Jefferson National Accelerator Facility, Newport News, VA

R. Dupre, M. Ouillon (co-spokesperson)
Laboratoire de Physique des 2 Infinis Irene
Joliot-Curie, University Paris-Saclay, Saclay, France

E. Cohen
Nuclear Research Center - Negev, Physics Dept., P.O. Box 9001, 84190 Beer-Sheva, Israel

(Dated: May 22, 2023)

## Executive Summary

Short-ranged correlated (SRC) nucleon-nucleon (NN) pairs are pairs of nucleons with large relative momentum ($p_{rel}$) and smaller center of mass momentum ($p_{cm}$). To date, SRC studies were based primarily on measurements of high-energy electron or proton scattering at large momentum transfer in direct kinematics off stable nuclei (e.g., $A(e,e'pN)X$). Such measurements break the SRC pairs and measure the emerging particles. However they are blind to the residual A-2 nuclear system.

Here we propose measuring the $^4$He$(e,e'pd)n$, $(e,e't)p$, and $(e,e'p)$ reactions at 6.4 GeV, detecting the scattered electron and proton in the CLAS12 forward detector and the low-momentum spectator deuteron (or triton) in the ALERT detector. By measuring or inferring all of the final state particles, we can measure both $\vec{p}_{rel}$ and $\vec{p}_{cm}$ and dramatically reduce the effect of final state interactions. This allows a unique fully exclusive study of $pn$-SRC in the $^4$He nucleus.

We will (1) test the critical assumption that the two body SRC pairs can be factorized from the residual nuclear system and (2) study the transition from single nucleons in a mean field (below the fermi level) to SRC pairs above the fermi level. In addition, we will perform the first study of the final states in the $^4$He$(e,e'p)$ reaction by measuring the $(e,e'p)X$, $(e,epd_S)n$, $(e,e'pt_S)$, and $(e,e't_S)p$ channels (where $S$ refers to a spectator). This will complement the higher statistics $(e,e'p)X$ and $(e,e'pN)X$ measurements of a wide range of nuclei in RGM.

The unique features of ALERT allow for a high-luminosity ($3\times10^{34}$ cm$^{-2}$s$^{-1}$) high-efficiency measurement of spectator deuteron and triton momenta between 100 and 300 MeV/c, covering most of the spectator nuclear fragment momentum distribution.

Because ALERT will be installed in CLAS12 in summer 2024 and the ALERT beam time will be scheduled well before then, this is the only opportunity to propose new ALERT experiments. We request 17 PAC days of beam time at 6.4 GeV on a $^4$He target.

**Contents**

## I. INTRODUCTION

Short-range correlations, pairs of nucleons with high relative and lower center-of-mass (cm) momentum, are an integral part of the nuclear medium. Nucleons at relatively short distances experience a strong tensor interaction, generating a high-momentum tail in the nuclear momentum distribution that extends significantly above the Fermi momentum. This high-momentum tail is a universal feature of atomic nuclei and of nuclear matter. Recent works have shown that short-range correlations (SRCs) account for approximately 20% of the nucleons in the nucleus and are predominantly neutron-proton pairs [1–12]. As nucleons are composite objects, their internal structure may well be modified when the distance between them is smaller than their radii, causing substantial overlap between their quark distributions [1]. SRC research therefore lies on the border between nuclear and bound-nucleon structure.

The short-range structure of nuclei is a vibrant field of research. Previous results have been published in Nature, Science, PRL, etc. SRC studies were also shown to have implications for many other topics, including quark distributions in nuclei (the EMC effect) and the free neutron structure [1, 13–17], nuclear symmetry energy and neutron star structure [5, 18–20], nuclear charge radii and the neutron skin of neutron-rich nuclei [21], energy sharing and correlations in ultra-cold two-component Fermi-gases [6, 22, 23], the analysis of low-energy ($\approx$ 50 MeV/A) heavy-ion collisions [18, 19], neutrino-nucleus interactions and the analysis of next-generation neutrino oscillation experiments [24, 25], pairing mechanisms and scale separation in nuclei [26, 27], and nuclear correlation functions and double beta decay [27, 28].

These results, and others, stimulated a significant theoretical effort that vastly improved our ability to model and calculate SRCs, and estimate their impact on various phenomena [26, 29–33]. The universality of the SRC pair momentum distribution (the fact that the momentum distribution of high-momentum nucleons has the same shape in all nuclei from deuterium to lead) depends on scale separation between the low-momentum scale of the mean-field nucleons (where the nucleon experiences the average potential of all the $A-1$ nucleons) and the high-momentum scale of the nucleons in SRC pairs (where the potential due to the other nearby nucleon is greater than the total potential due to the other nucleons). This scale separation predicts that the directions of $\vec{p}_{rel}$ and $\vec{p}_{cm}$ should be uncorrelated.

### A. Theoretical Interpretation

The study of short-range correlations is a broad subject, covering a large body of experimental and theoretical work, as well as phenomenological studies of the implications of SRCs for other phenomena in nuclear, particle, and astro-physics. A full discussion of SRC physics is available in a RMP review [1] and a theory-oriented review [2].

The results presented below are based on measurements of high-energy electron scattering in large-momentum-transfer kinematics (i.e., hard scattering). These measurements' resolving power is determined by their momentum transfer, and their interpretation relies on the theoretical modeling of the interaction. The latter should account for all possible reaction mechanisms that lead to the same measured final state. High-momentum transfer measurements can therefore be viewed in several ways. The discussion below views the electron interaction in terms of Quasi-Elastic (QE) scattering off single nucleons, which is the simplest reaction picture that is consistent with both the measured observables [1, 2, 4, 5] and various reaction and ground-state ab-initio calculations [3, 34]. Nuclei can also be described in a picture in which the probe interacts with a simpler ground state, though with more complex short-distance multi-nucleon operators. In this case, the complexity of the wave function is converted to the complexity of the operators through a unitary transformation [35]. While we discuss the proposed measurements in the first picture, the two pictures are physically equivalent.

### B. Experimental Results

Over the last decade, we have learned a remarkable amount about SRCs, obtained from measurements of exclusive hard knockout reactions, $A(e, e'p)$ and $A(e, e'pN)$ [6–8, 36–38] (here $N$ stands for neutron or proton), primarily from selected nuclei ($^3$He, $^4$He, C, Al, Fe, and Pb). The electrons in these reactions interacted with protons or neutrons in the target nucleus via a high-momentum transfer reaction ($Q^2 \geq 1.2$ GeV$^2$), leading to the knockout of a high-momentum nucleon and, in certain events, the simultaneous emission of a correlated recoil nucleon. This correlated recoil nucleon is a 'spectator' to the interaction.

Exclusive measurements of SRC pair breakup reactions using hadronic (proton) [9, 39] and electronic [6, 8, 40, 41] probes on various nuclei (see Fig. 1) found that:

- All high-missing momentum ($300 \leq p_{miss} \leq 600$ MeV/c where $\vec{p}_{miss} = \vec{p}_p - \vec{q}$) knocked-out protons have an associated recoil nucleon with a momentum that balances the missing momentum.
- These recoil nucleons are almost entirely neutrons. Neutron-proton ($np$) pairs are nearly 20 times more prevalent than proton-proton ($pp$) pairs, and by inference, neutron-neutron ($nn$) pairs.
- The relative momenta of the SRC pairs are higher than $k_F$, while the cm momenta are consistent with the total momentum of two mean-field nucleons ($k_F$ is the nuclear Fermi momentum, typically about 250 MeV/c for medium to heavy nuclei).

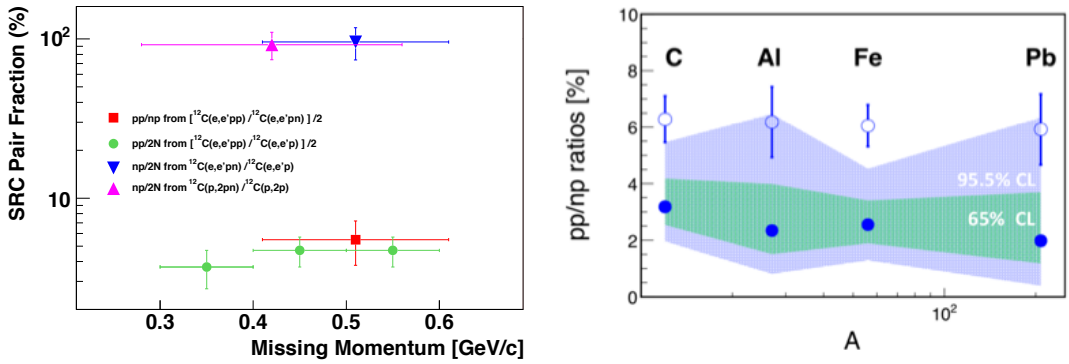


**FIG. 1:** Results on $np$-SRC dominance in nuclei from $^4$He to Pb from $A(p, 2p)$, $A(e, e'p)$ and $A(e, e'pN)$ measurements. Left: fraction of knocked-out protons with a correlated neutron (triangles) or proton partner (green circles), and the ratio of $pp$- to $np$-SRC pairs (red squares) in C, extracted from $(p, 2pn)$ [9, 39] and $(e, e'pN)$ [6–9, 39, 40] measurements; Right: the ratio of $pp$ to $pn$ SRC pairs for different nuclei from $(e, e'pN)$ measurements [41], before (open circles) and after (filled circles) correcting for reaction mechanism effects. The inner and outer bands represent the 68% and 95% confidence limits of the corrected ratios, respectively.

### C. SRC Theory

From a theoretical standpoint, the dominance of $np$-SRC pairs over $pp$-SRC pairs in nuclei has been primarily studied using state-of-the-art ab-initio many-body calculations

of pair momentum distribution functions for different nuclei [2, 42–46]. These calculations show the dominance of $np$ pairs at relative pair momenta greater than 300 MeV/c. By considering different variations of the $NN$ interaction, for example with and without a significant tensor force, the unique role of the tensor force in the relevant momentum range can be identified [42].

The 'generalized contact formalism' (GCF) approach exploits the underlying dynamics of SRC pairs in nuclei [26]. In this approach, the short-distance many-body wave function factorizes into a universal two-body function that depends only on the pair relative momentum ($q$ or $p_{rel}$), times a 'mean-field like' many-body function that depends on the pair cm momentum ($Q$ or $p_{cm}$). This factorization stems from the scale separation between high-momentum, short-distance scales, responsible for the pair relative momentum, and lower-momentum, longer-distance scales associated with the nuclear many-body dynamics affecting the total number of pairs and their cm momentum distribution. This new formalism was successfully bench-marked against state-of-the-art VMC (variational Monte Carlo) and Cluster-VMC calculations of nuclei from $^4$He to $^{40}$Ca in both momentum and coordinate space [26]. This phenomenological approach was validated by more detailed theoretical calculations [30] which showed that the pair-based GCF calculations agreed remarkably well with ab-initio Quantum Monte Carlo calculations of nuclei from deuteron to $^{40}$Ca.

One key aspect of this scale separation is that since $\vec{p}_{cm}$ and $\vec{p}_{rel}$ arise from different momentum and distance scales, they are independent of each other. This implies that $\vec{p}_{cm}$ and $\vec{p}_{rel}$ should be completely uncorrelated.

## II. PHYSICS GOALS

The studies of SRC were based so far primarily on measurements of high-energy electron/proton scattering at large momentum transfer in direct kinematics off stable nuclei. Such measurements break the SRC pairs and measure the emerging particles, both the struck nucleon and its partner spectator (recoil) nucleon. However they are blind to the residual A-2 nuclear system. Here we propose measuring the $^4$He$(e, e'pd)n$ reaction using 6.4 GeV electron beam and the ALERT detector. This allows a unique fully exclusive study of $pn$-SRC in the $^4$He nucleus. We plan to detect the $p$ and $d$ and reconstruct the $n$ from the missing energy and momentum.

The motivation for this fully exclusive measurement is twofold:

1. Test the basic assumption that the two body SRC pairs can be factorized from the residual nuclear system and

2. Study the transition from the single nucleons in a mean field (typically below the Fermi momentum) to SRC pairs (typically above the Fermi momentum).

### A. SRC Factorization Test

The strong two-body interaction between the nucleons in a short-range pair was predicted [30, 47] to allow describing SRC momenta as the product of a universal (i.e., nucleus-independent) function of $\vec{p}_{rel}$ with a nucleus-dependent function of $\vec{p}_{cm}$, with no correlation between them. Such factorization dramatically simplifies the SRC calculations. This factorization should be evident experimentally by a lack of correlation between $\vec{p}_{rel}$ and $\vec{p}_{cm}$.

Unfortunately, there is only one low-statistics measurement of this angular correlation [48]. They measured the $^{12}\mathrm{C}(p, 2p^{10}B)n$ reaction in inverse kinematics at the Joint Institute for Nuclear Research (JINR), using a 48 GeV/c $^{12}$C beam incident on a hydrogen target. By detecting the $^{10}$B recoil they dramatically reduced the impact of nucleon rescattering (final state interactions or FSI), inferred the recoil neutron, and measured $\vec{p}_{cm} = \vec{p_B}$ directly, rather than reconstructing $\vec{p}_{cm}$ by combining three much larger vectors ($\vec{p}_{cm} = \vec{p}_{p_1} + \vec{p}_{p_2} - \vec{p}_{beam} + \vec{p}_n$, where $p_{p_1} > p_{p_2}$ (i.e., $p_1$ is the leading proton) and all quantities are calculated in the incident $^{12}$C rest frame).

Fig. 2 shows the distribution of the cosine of the angle between the $^{10}$B momentum ($\vec{p}_{cm} = \vec{p_B}$) and the pair relative momentum given by $\vec{p}_{rel} = (\vec{p}_{miss} - \vec{p_n})/2$ where $\vec{p}_{miss} = \vec{p}_{p_1} + \vec{p}_{p_2} - \vec{p}_{beam}$ and all quantities are calculated in the incident $^{12}$C rest frame). The data is compared to the GCF simulation, which assumes factorization and therefore predicts a flat distribution (which is slightly shaped by the acceptance of the detectors). The agreement shows that $\vec{p}_{cm}$ and $\vec{p}_{rel}$ are uncorrelated, although with low statistical confidence due to the paltry 21 events.

This experiment is kinematically very similar to the proposed measurement, in that both detected the scattered probe, the struck proton, and the residual $A-2$ nucleus, and then inferred the undetected neutron using missing mass. In the JINR experiment, they used

inverse kinematics so that they could detect the $A = 10$ and $A = 11$ nuclear recoils at high-momentum in the lab frame. We propose to use ALERT to detect low-momentum $d$ and $t$ recoils.

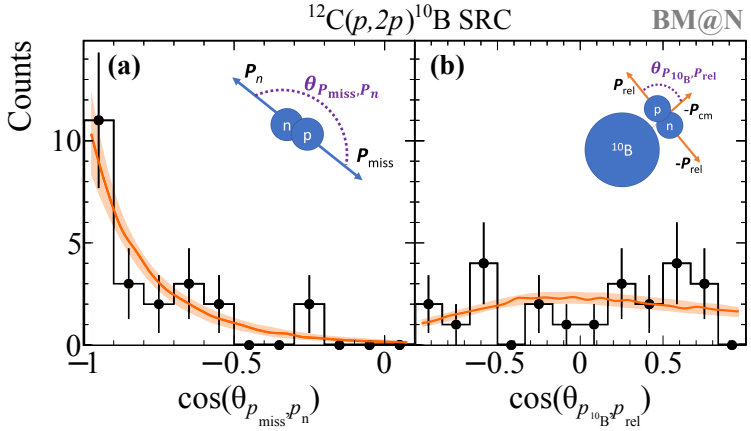


**FIG. 2:** Distributions of the cosine of the angle between (a) the recoil nucleon and the missing momentum and (b) the $^{10}$B recoil and the pair relative-momentum. Data (black points) are compared with GCF predictions (orange lines). The width of the bands and the data error bars show the systematic uncertainties of the model and the statistical uncertainties of the data, respectively, each at the $1\sigma$ confidence level. Figure taken from Reference [48].

Measuring the $^4$He$(e, e'pd)n$ reaction using a 6.4 GeV electron beam, CLAS12 and the ALERT detector can probe $pn$-SRC pairs by detecting the $p$ and $d$ and reconstructing the $n$. This will allow us to reconstruct neutrons at all momenta and angles. This is a complete kinematic measurement that will allow us to reconstruct $\vec{p}_{cm}$ and $\vec{p}_{rel}$.

### B. Mean-field SRC Transition

A complete high-resolution microscopic description of atomic nuclei should have a nucleus-dependent mean field and long-ranged nuclear shell model parts as well as explicit nucleus-independent SRC-pair parts. Effective theoretical models describe well the dynamics of nucleons at the high- and low-momentum regimes of the nuclear distribution. However, for a full description of the nucleus, the transition region between the two regimes needs to be understood. The experimental challenge of mapping this transition is the need to detect

the low momentum recoil nucleon, which is quite difficult.

High-energy, large-momentum-transfer triple-coincidence measurements at EVA/BNL [9] measured the neutron distribution for the $C(p, 2p+n)X$ reaction in quasi-elastic kinematics (see Fig. 3). They measured the opening angle $\gamma$ between the neutron momentum ($\vec{p}_n$) and the missing momentum ($\vec{p}_{miss} = \vec{p}_{beam} - \vec{p}_{p_1} - \vec{p}_{p_2}$) as a function of $|\vec{p}_n|$. They found no correlation for $p_n \leq p_F \approx 220$ MeV/c. However, for $p_n \geq p_F$ (i.e., the SRC regime), the neutrons were all emitted in the backward hemisphere relative to $\vec{p}_{miss}$.

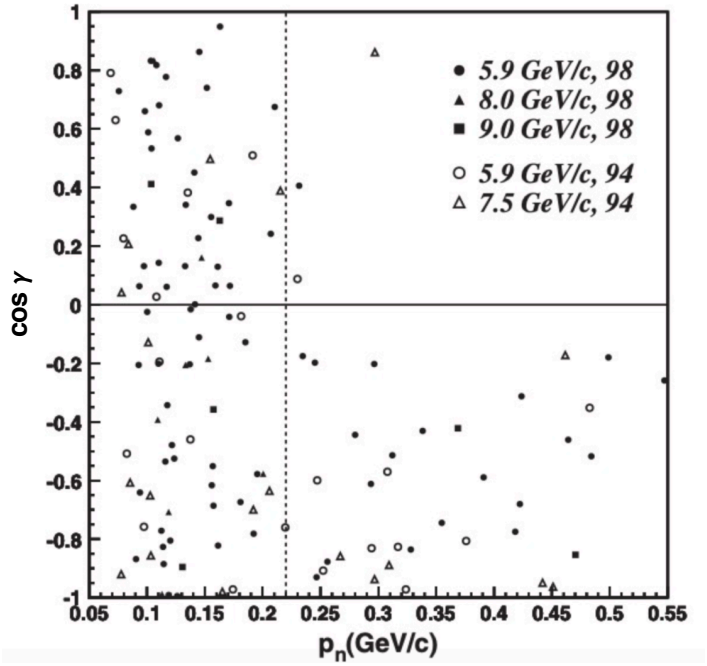


**FIG. 3:** Cosine of the opening angle $\gamma$ between the neutron momentum $\vec{p}_n$ and $\vec{p}_{miss}$ as a function of $p_n$ from measurements of the $C(p, 2p+n)X$ reaction in quasi-elastic kinematics. The dotted vertical line shows the carbon Fermi momentum $p_F = 220$ MeV/c. Figure taken from Reference [9].

Thus the data indicate the existence of a clear transition in the nuclear response around the Fermi momentum, with SRC dominance at high momenta. However, again the low statistics of the hadronic data limit our ability to quantify the width (i.e., the abruptness) of this important transition.

A 5.0-GeV CLAS measurement [49] of the per-nucleon $C(e, e'p)$ cross-section ratio for carbon to deuterium as a function of $p_{miss}$, integrated over $0.7 \leq x_B \leq 1.8$, also shows a

transition from independent particle to SRC degrees of freedom, see Fig. 4. The data agrees nicely with a single particle calculation for $p_{miss} \leq p_F$ and with an SRC calculation for $p_{miss} \geq 400$ MeV/c. In between there is a relatively narrow transition region.

However, this attempt to map the mean field to SRC transition relies on model dependent calculations. The proposed measurement will allow us to extract the transition model independently, as done for the BNL C$(p, ppn)$ measurement, but with far better statistics. We will plot the neutron-$p_{miss}$ opening angle versus the neutron momentum to map out this transition more precisely.

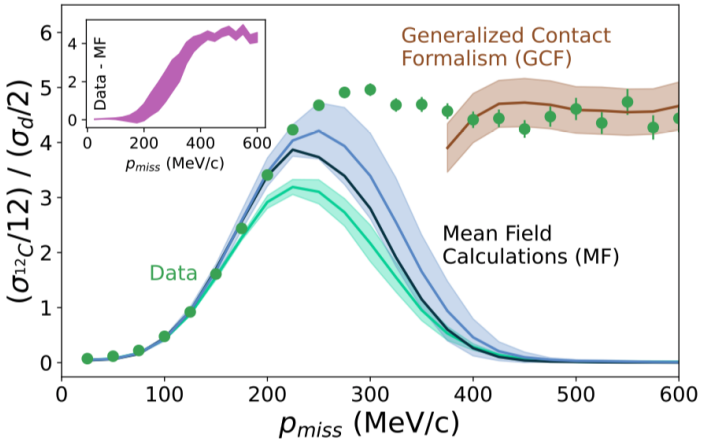


**FIG. 4:** The per nucleon $(e, e'p)$ cross-section ratio for carbon to deuterium as a function of $p_{miss}$, integrated over $0.7 \leq x_B \leq 1.8$. Filled circles show the data. The teal, black, and azure lines show the calculated cross sections obtained using QMC (teal), IPSM (black), and Skryme (azure) based one-body mean-field models for nucleon distributions in carbon. The brown line shows a GCF calculation for SRC nucleons in carbon. The insert shows the result of subtracting the mean-field calculations from the carbon data. The widths of the bands indicate the corresponding $1\sigma$ uncertainties in the calculations. Figure taken from Reference [49].

It is important to determine the width and nature of this transition region. If the transition region is narrow, then we can construct three-region high-precision nuclear models for heavy nuclei which are still beyond the reach of modern "exact" *ab initio* calculations. These models would have a nucleus-dependent mean-field region at low nucleon momenta, a

nucleus-independent SRC region at high momenta, and a more complicated transition region between. If the transition is broad, then these three-region models will not work as well. In addition, this measurement will determine the regions of applicability of the mean-field and SRC models.

### C. Residual-nuclear Final States in $(e, e'p)$

Lastly, this experiment will determine the probability of different $A-1$ final states for proton knockout from $^4$He. It will do this by detecting the $(e, e'p)$, $(e, e'pd_S)n$, and $(e, e't_S)p$ reactions and determine the relative probability of $pt$, $pnd$ and $ppnn$ final states. These will help guide theorists calculating this reaction.

## III. EXPERIMENTAL SETUP AND RATE ESTIMATES

### A. Experimental Setup

We plan to measure the $^4$He$(e, e'p)$, $(e, e'pd_S)n$, and $(e, e't_S)p$ reactions at 6.4 GeV in Hall B, detecting the scattered electron and knocked-out proton in the CLAS12 Forward Detector (FD) [50] and the spectator deuteron and triton in ALERT (A low energy recoil tracker). We will use nominal torus and solenoid magnetic fields. The Moller cone will be installed to reduce backgrounds.

The ALERT detector [51] replaces the standard CLAS12 central tracker and detects recoil particles down to low energies. It consists of two sub-systems: a drift chamber and a scintillator hodoscope, see Fig. 5. ALERT has an azimuthal acceptance of about 340°, uncorrelated with its momentum and polar angle acceptances. The active area of ALERT extends out to a radial distance of about 10 cm. The drift chamber will be composed of eight layers of sense wires to provide tracking information, while the scintillators will provide particle identification through time-of-flight and energy measurements, see Fig. 6(bottom right). For more details see Ref. [51]. Protons, deuterons, tritons and $^3$He are clearly separated. Deuterons will be separated from $^4$He using energy deposition in the drift chamber and scintillators, and by using baryon conservation. Angular and momentum resolutions are shown in Fig. 6.

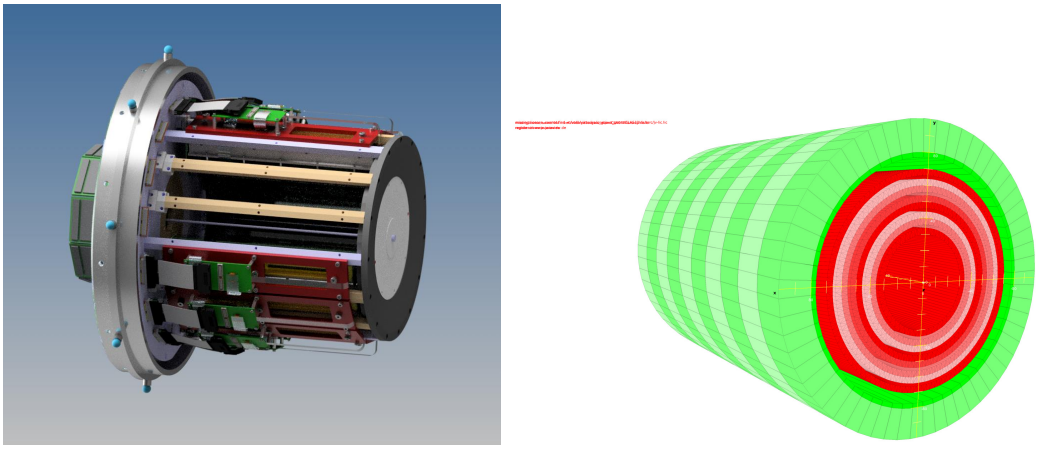

**FIG. 5:** (left) Engineering drawing of the assembled ALERT detector. (right) Drawing of the ALERT detector showing the drift chambers (red) and scintillators (green). Figures from Ref. [51].

In order to maximize luminosity, the drift chamber will be operated at relatively low gain so that minimum ionizing particles will not be detected. ALERT covers a deuteron momentum range from 100 to at least 300 MeV/c with high efficiency (for more details see Sec. III B 6). We will use ALERT in its standard configuration.

The CLAS12 forward detector (FD) will be used in its standard configuration. It consists of drift chambers for tracking, a high-threshold Cherenkov counter (HTCC), scintillation counters (FTOF) for time-of-flight measurement, and a preshower (PCAL) and forward calorimeters (ECAL). We will use the standard electron-only trigger with a calorimeter threshold of about 1 GeV. These settings have been used by many CLAS12 run groups such as Run Group F and Run Group M (RGM).

The target is a 35-cm long, 6-mm diameter straw filled with $^4$He at 3 atm, corresponding to an areal density of about 17 mg/cm$^2$. We plan to run at the predicted 11-GeV ALERT luminosity of $3 \cdot 10^{34}\,\text{nucleons}\,\text{cm}^{-2}\,\text{s}^{-1}$ [51], which corresponds to a beam current of about 500 nA. Backgrounds will be reduced by operating the drift chamber at low gain (to reduce signals from minimum ionizing particles and neutrals) and by $z$-vertex matching between tracks in the FD and ALERT in the 35-cm target. We expect the backgrounds to be lower at our proposed 6.4 GeV energy, than at 11 GeV.

We will reconstruct the undetected neutron in the $(e, e'pd)n$ reaction using missing mass. The dominant momentum uncertainty of about 60 MeV/c comes from the $\approx 1\%$ electron

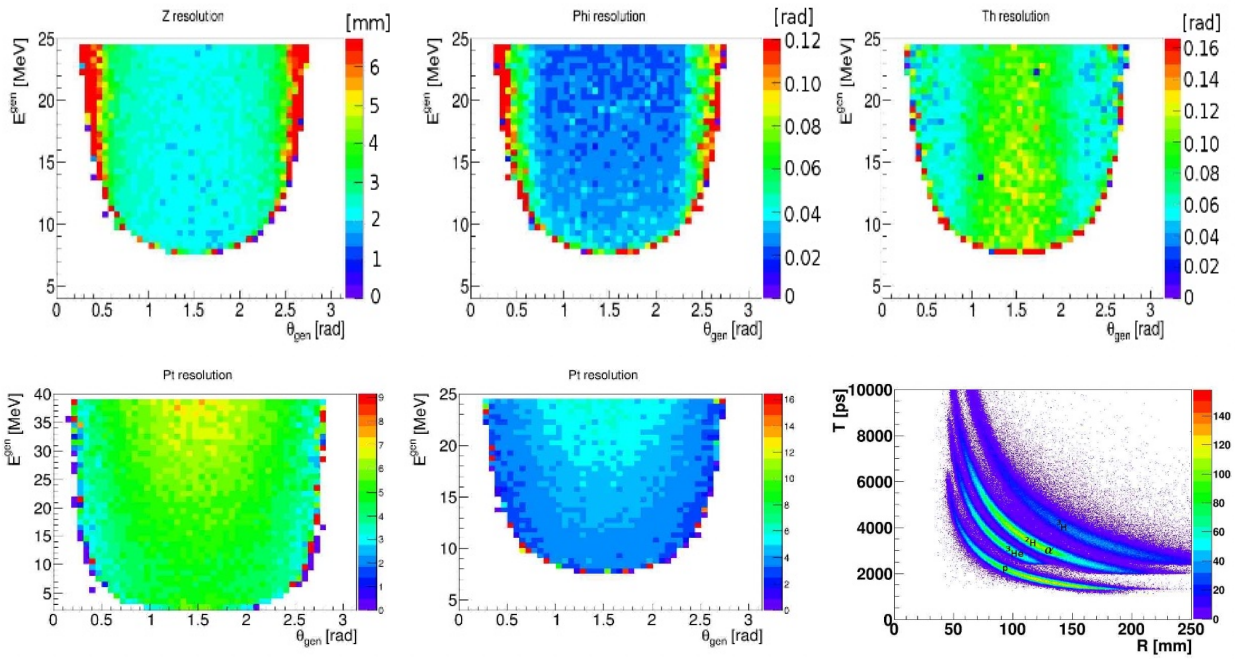


**FIG. 6:** (top) Expected ALERT resolution in $z$-vertex (left), $\phi$ (middle) and $\theta$ (right) for $^4$He nuclei as a function of $^4$He kinetic energy and angle; (bottom) Expected ALERT momentum resolution (in percent) as a function of particle kinetic energy and angle for protons (left) and for $^4$He nuclei (middle). (right) Simulated time of flight at the scintillator versus the reconstructed radius (corresponding to measured momentum) in the drift chamber for various recoil nuclei (from the bottom, the bands correspond to $p$, $^3$He, $^4$He/$d$, $^3$H). Figures from Ref. [51].

momentum resolution. Uncertainties in the proton ($\approx 1\%$) and deuteron momentum (see Fig. 6) measurements will increase the overall uncertainty in the reconstructed neutron momentum to about 80 MeV/c. This resolution will be good enough to easily identify the missing neutrons. We will take this width into account when measuring the transition from mean-field to SRC as a function of neutron momentum.

## B. Rate Estimations

### 1. *Overview*

The scattered electron and leading proton from the $^4$He$(e, e'pd_s)n$ reaction will be detected in the CLAS12 Forward Detector. We used 6-GeV RGM $^4$He$(e, e'p)$ data using the same

FD configuration to estimate rates for this proposal. RGM could not measure spectator deuterons using the standard CLAS12 central vertex trackers (which cannot detect low momentum particles due to the high solenoid magnetic field and to energy loss in the silicon vertex detector).

We inferred the number of $^4\mathrm{He}(e,e'pd_s)n$ events from the measured number of RGM $^4\mathrm{He}(e,e'p)$ events with a proton in the FD by assuming that all high-$p_{miss}$ events had a correlated recoil neutron and an isotropic spectator $d$. We used the measured SRC-pair $p_{cm}$ distribution [52] for the deuteron momentum distribution. We then corrected this for the ALERT deuteron acceptance and added a conservative factor for the probability that the deuteron is emitted intact from the nucleus and that there was no $pn$ rescattering.

The following sections introduce some kinematic quantities of the reaction, show the RGM SRC event selection and the deuteron acceptance of ALERT. At the end we determine the expected number of events and and the required beam time.

### *2. Kinematic Variables*

The standard electron scattering quantities are

$$Q^2 = |\vec{q}|^2 - \omega^2, \tag{1}$$

$$x_B = \frac{Q^2}{2\omega m_N} \tag{2}$$

with 3-momentum transfer $\vec{q} = \vec{p}_e - \vec{p'}_{e'}$, energy transfer $\omega = E - E'$, and $m_N$ is the nucleon mass.

The outgoing proton which absorbs the virtual photon is called the "leading" proton and has momentum $\vec{p}_p$.The missing momentum is:

$$\vec{p}_{miss} = \vec{p}_p - \vec{q} \tag{3}$$

so that $\vec{p}_{miss}$ is parallel to the initial proton momentum (in the absence of final state interactions). The missing mass assuming electron scattering from a stationary correlated nucleon pair at rest is defined as (ignoring the binding energy of the pair):

$$M^2_{miss} = (\omega + m_d - E_p)^2 - |\vec{q} - \vec{p}_p|^2 \tag{4}$$

with $pn$ pair mass equal to the deuteron mass $m_d$, and proton energy $E_p$. We use this missing mass in the analysis of RGM data to cut out inelastic scattering events. We also

define the following angles with respect to $q$:

$$\theta_{pq} = \angle(\vec{p}_p, \vec{q}), \tag{5}$$

$$\theta_{p_{miss}q} = \angle(\vec{p}_{miss}, \vec{q}). \tag{6}$$

### *3. Event Selection*

We require that the electron and leading proton are detected in the CLAS12 forward detector using the standard RGM PID. This includes sampling fraction cuts (both in ECAL energy loss and momentum, see Fig. 8) and a conservative PCAL distance to edge cuts (see Fig. 7) for electrons and $\chi^2$pid cuts for protons (see Fig. 9).

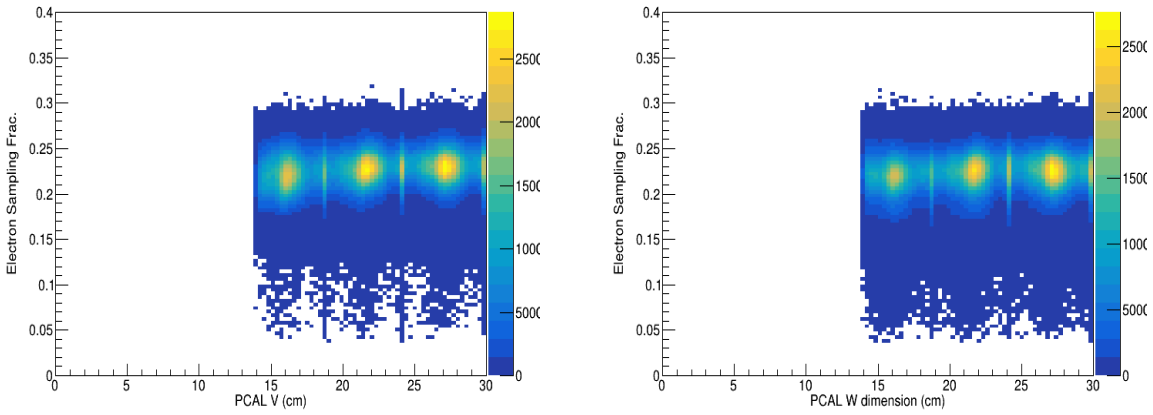


**(a)** v direction cut **(b)** w direction cut

**FIG. 7:** PCAL edge cuts

To select quasi-elastic events, we require $Q^2 > 1.2\,\mathrm{GeV}^2/c^4$ to select "hard" reactions and to suppress non quasi-elastic reaction channels such as meson-exchange. An added advantage of measuring at large $Q^2$ is that the struck (leading) proton has high momentum. To identify leading protons, we require that the knocked-out proton be emitted within a 25° cone of the momentum transfer vector, $\theta_{pq} \leq 25°$, and that $|p_p|/|q| > 0.6$ to ensure that the proton carries a large fraction of the momentum transfer and was the one that absorbed the virtual photon.

We cut on $M_{miss} < 1.03\,\mathrm{GeV}/c^2 < m_p + m_\pi$ (where $m_\pi$ is the pion mass) to suppress inelastic contributions such as pion production. Fig. 10 shows the distribution of $M_{miss}$

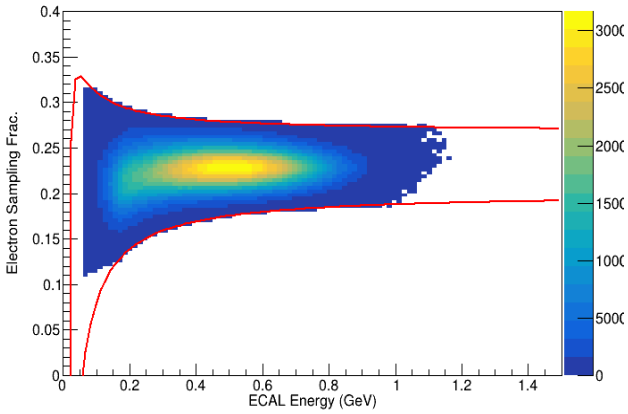


**FIG. 8:** Sampling Fraction vs ECAL energy loss cuts

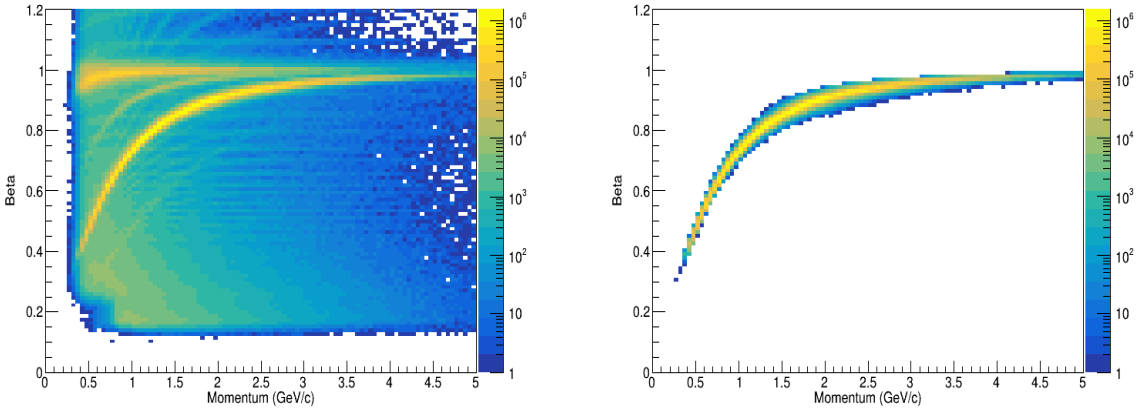


**(a)** All positive particle PID

**(b)** Proton PID selection $\chi^2 < 3$

**FIG. 9:** Proton particle identification

versus $x_B$ for all events with $Q^2 > 1.2\,\mathrm{GeV}^2/c^4$, $\theta_{pq} \leq 25°$, and $|p_p|/|q| > 0.6$ cuts. The horizontal red line indicates the $M_{miss}$ cut.

Fig. 11 shows the distribution of all protons with $Q^2 > 1.2\,\mathrm{GeV}^2/c^4$ and $m_{miss} < 1.03\,\mathrm{GeV}/c^2$. The low $p_{miss}$ protons are located at small $\theta_{pq}$ with $p/q \approx 1.05$ and the higher $p_{miss}$ protons form a tail extending to larger $\theta_{pq}$.

These cuts are similar to those used in previous SRC analyses [6, 53–55]. However, these cuts do not include either an $x_B$ cut or a missing momentum cut; this allows us to detect both mean-field and SRC knock-out events.

Next, we looked at the angular and momentum distributions of the electron and leading

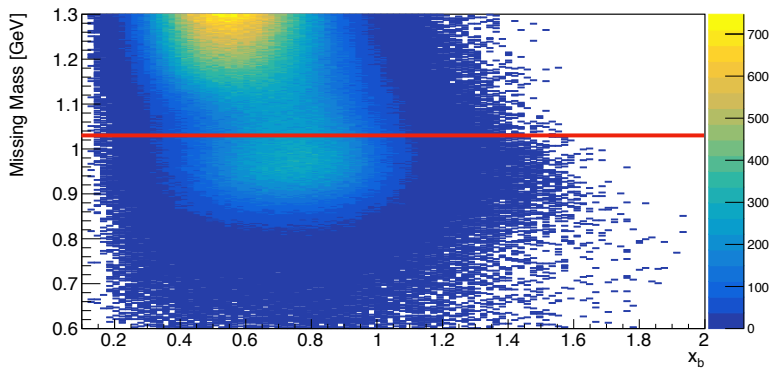


**FIG. 10:** Distribution of $m_{miss}$ as a function $x_B$ for events with $Q^2 > 1.2$ GeV$^2$, $\theta_{pq} \leq 25^\circ$, and $|p_p|/|q| > 0.6$ and an electron and proton in the forward detector. The horizontal red line indicates the missing mass cut applied in the event selection for the rate estimate of this proposal.

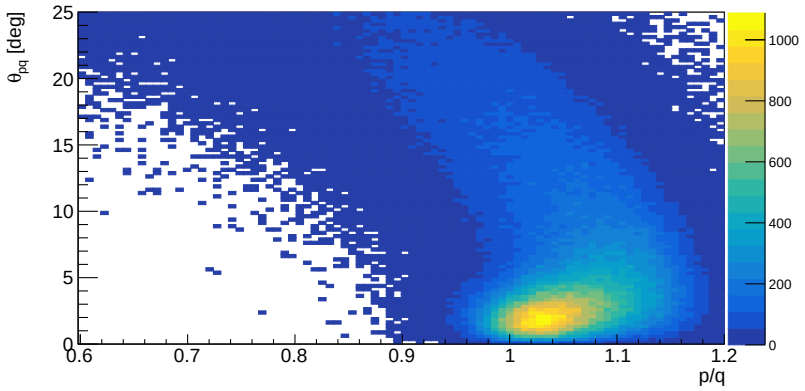


**FIG. 11:** Distribution of the angle between the leading proton and $\vec{q}$ as a function of the momentum ratio $|p_p|/|q|$ for events with $Q^2 > 1.2$ GeV$^2$, $m_{miss} < 1.03\,\mathrm{GeV}/c^2$, and an electron and proton in the forward detector.

proton. These are shown in Fig. 12 with $Q^2 > 1.2$ GeV$^2$, $\theta_{pq} \leq 25^\circ$, $|p_p|/|q| > 0.6$ and $m_{miss} < 1.03\,\mathrm{GeV}/c^2$ cuts. We can clearly see the 6-fold structure of the CLAS12 detector. The proton angular distributions have some events for $\theta_p \approx 40^\circ$ where those protons pass through the mass of the central detector before being detected in the FD. We cut out those events, requiring $\theta_p \leq 37^\circ$.

Fig. 13 shows the correlation between $p_{miss}$ and proton angle $\theta_p$. The applied cut of

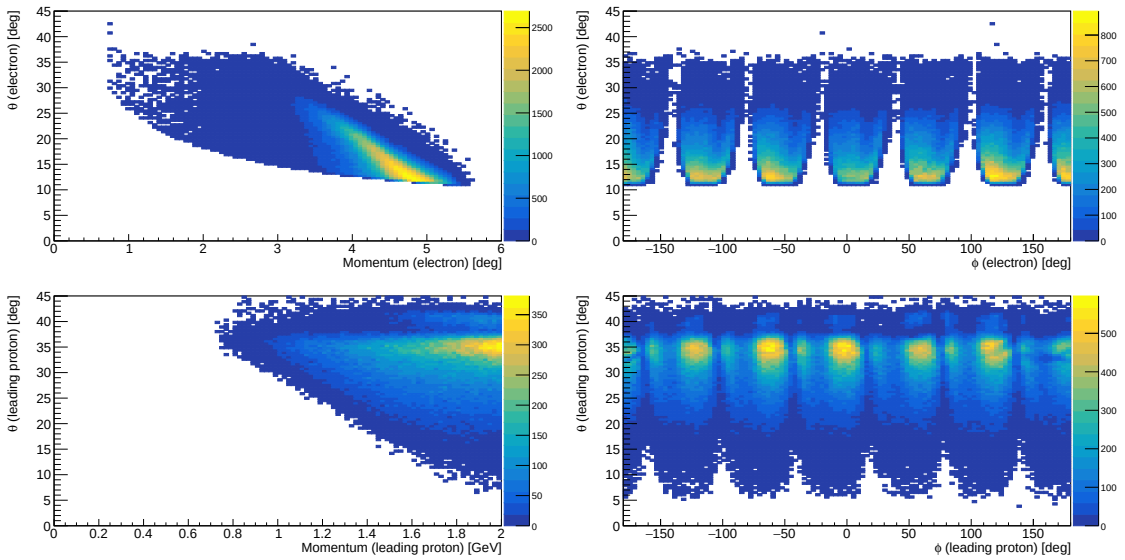


**FIG. 12:** Momentum and angular distributions for the electron and leading proton for events with the cuts $Q^2 > 1.2$ GeV$^2$, $\theta_{pq} \leq 25°$, $|p_p|/|q| > 0.6$ and $m_{miss} < 1.03\,\mathrm{GeV}/c^2$. (Top left) electron momentum versus $\theta$. (Top right) electron $\theta$ versus $\phi$. (Bottom left) proton momentum versus $\theta$. (Bottom right) proton $\theta$ versus $\phi$.

$\theta_p < 37°$ is shown by the red line. This cut does not restrict the $p_{miss}$ range of the data.

Finally, we use the $\theta_{p_{miss},q}$ versus $p_{miss}$ distribution to estimate the number of events in the SRC region from the RGM data. The distribution is shown in Fig. 14. We estimate the number of SRC $(e, e'p)$ events by requiring $p_{miss} \geq 400\,\mathrm{MeV/c}$ (marked by the red box). This is justified by the simulations as described in Section III B 5.

The total number of RGM SRC events for $p_{miss} > 400\,\mathrm{MeV/c}$ is $3.8 \times 10^5$ at a luminosity of $1.2 \cdot 10^{35}\mathrm{cm}^{-2}\mathrm{s}^{-1}$ and a running time of 4 PAC days.

### *4. Minimizing Final State Interactions*

The leading proton in the $(e, e'p)$ reaction can rescatter from other nucleons as it leaves the nucleus (referred to as final state interactions or FSI). There are two general classes of FSI. In the first class, scattering from a low-momentum (mean-field) proton can result in large $p_{miss}$. In these events the virtual photon is absorbed on a mean field proton,

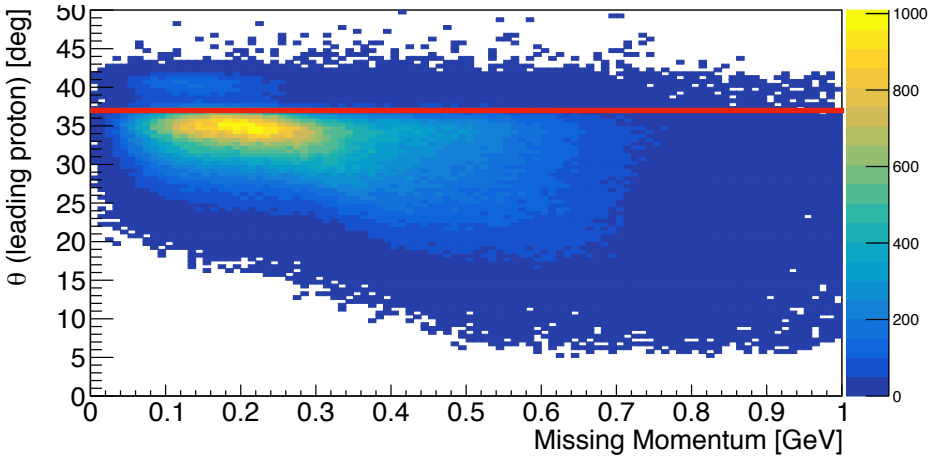


**FIG. 13:** Number of $(e, e'p)$ events plotted as a function of $\theta_p$ and $p_{miss}$ for events with $Q^2 > 1.2$ GeV$^2$, $\theta_{pq} \leq 25°$, $|p_p|/|q| > 0.6$, and an electron and proton in the forward detector. The horizontal red line indicates the cut on $\theta_p$.

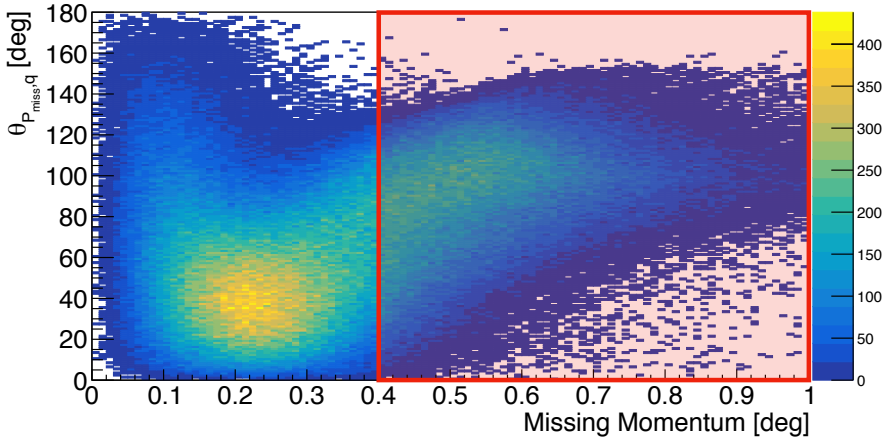


**FIG. 14:** Distribution of $\theta_{p_{miss},q}$ as a function $p_{miss}$ for $(e, e'p)$ events with $Q^2 > 1.2$ GeV$^2$, $\theta_{pq} \leq 25°$, $|p_p|/|q| > 0.6$, and an electron and proton in the forward detector ($\theta_p \leq 37°$). The red box marks the area used for the data-based SRC count estimate for this proposal.

which then rescatters from a neutron, resulting in a *pnd* final state and a larger $p_{miss}$. Non relativistically, when a particle scatters from an equal-mass particle, the two particles have an opening angle of 90°. Relativistically, when a high-momentum proton scatters from a low-momentum neutron, the lab-frame opening angle $\theta_{pn}$ will be centered between 70° and

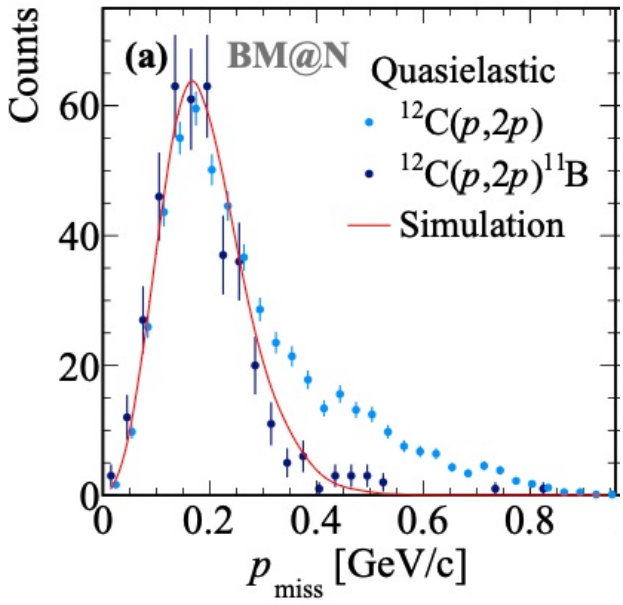


**FIG. 15:** Missing-momentum distribution in 12C rest-frame for quasielastic $^{12}\mathrm{C}(p,2p)$ (light blue) and $^{12}\mathrm{C}(p,2p)^{11}\mathrm{B}$ (dark blue) events. Solid red line shows the result of a quasielastic reaction simulation. Figure from [48]

90° with a width depending on the neutron momentum distribution. In order to minimize the effect of these interactions, we will cut out events with $\theta_{pn}$ in this range. This will reduce the expected number of events. Note that we cannot evaluate use this factor using the RGM data, since we cannot yet detect or reconstruct the neutron reliably in the central detector.

In the second class of FSI events, the electron scatters from a high-$p_{miss}$ proton, leaving a recoil partner neutron and a spectator deuteron. The proton then rescatters from the deuteron. Because the deuteron is so loosely bound, this high-momentum *pd* rescattering will typically break up the deuteron, leaving a *ppnn* final state. We will minimize the effect of these interactions by requiring a *pnd* final state.

A similar cut on the residual nuclear system was made in the JINR $\mathrm{C}(p,pp)$ measurement performed in inverse kinematics (i.e., with an incident 48 GeV/c C beam incident on a hydrogen target). The $(p,2p)$ missing momentum distribution had a large contribution at high-$p_{miss}$ due to inelastic and rescattering events (see Fig. 15). By requiring an intact $^{11}$B recoil, they dramatically reduced the effect of inelastic reactions and rescattering, as seen by the agreement between the $^{12}\mathrm{C}(p,2p)^{11}\mathrm{B}$ events and the simulation assuming single-nucleon

knockout without rescattering.

### 5. *Validation of RGM Data with Quasi-elastic Simulation*

We have validated our analysis of RGM data using a Monte Carlo simulation of quasi-elastic $^4$He$(e,e'p)$ events. The Monte Carlo event generator uses the Plane-Wave Impulse Approximation (PWIA) to write the scattering cross section in terms of a nuclear spectral function:

$$\frac{d^6\sigma}{d\Omega_e dE_e d\Omega_p dE_p} = p_p E_p \sigma_{ep} \mathcal{S}(p_{miss}, E_{miss}), \tag{7}$$

where $\Omega_e$ and $E_e$ are the outgoing angles and energy of the scattered electron, $\Omega_p$, $E_p$, and $p_p$ are the outgoing angles, energy, and momentum of the knocked-out proton, $\sigma_{ep}$ is the off-shell electron-proton cross section, and $\mathcal{S}$ is the spectral function, which defines the probability of finding a proton within the nucleon with momentum equal to $p_{miss}$, and separation energy equal to $E_{miss}$. In our simulation, we have used the cc1 prescription of Ref. [56] for $\sigma_{ep}$, and the form factor parameterization of Ref. [57] for the proton's on-shell form factors. We used the $^4$He spectral function calculated by N. Rocco and A. Lovato using Variational Monte Carlo techniques [58]. The calculation includes both $^4$He$(e,e'p)t$ and $^4$He$(e,e'p)nd$ break-up channels, but only includes information on the momentum of the proton (i.e., there is no information on the distribution of the $n$ and $d$).

We applied a very similar set of event selection criteria to the simulated Monte Carlo events as we applied to data. To roughly mimic the acceptance of the CLAS12 forward detector, we required both the electron and proton have scattering angles ($\theta_e$, $\theta_p$) between 5° and 37°. We further required:

- $Q^2 > 1.2$ GeV$^2$,
- $0.2 < x_B < 2.0$,
- $\theta_{pq} < 25°$,
- $M_{miss} < 1.03$ GeV, and
- $|p|/|q| > 0.6$.

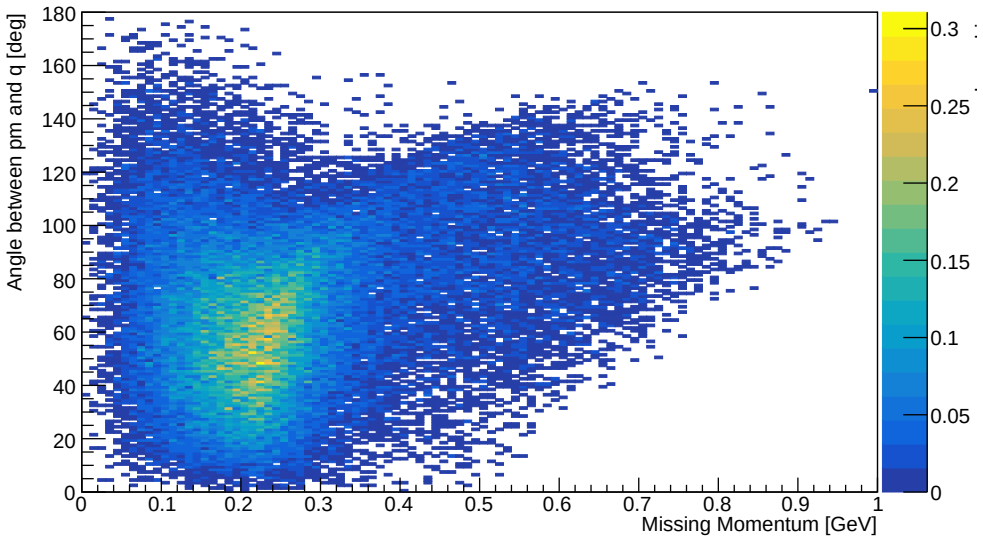


**FIG. 16:** Simulated distribution of $p_{miss}$ vs. the angle between $\vec{p}_{miss}$ and $\vec{q}$ for events passing the event selection criteria. Missing momentum resolution of about 80 MeV/c is not included.

The kinematic distributions are quite similar between the data (Fig. 14) and the simulation (Fig. 16). Both have a peak at $p_{miss} \approx 0.2$ GeV/c and $\theta_{p_{miss}q} \approx 40°$ and an extended distribution at higher $p_{miss}$ and higher $\theta_{p_{miss}q}$. The qualitative similarity indicates that the kinematic cuts on the data are selecting quasi-elastic events. Differences between the two distributions are likely due to FSI, which will be removed using a cut on the opening angle between the proton and neutron discussed above.

In addition, because the simulation used a detailed spectral function, we can see the expected final states as a function of missing momentum. Small missing momentum events are dominated by two-body *pt* breakup and large missing momentum events are dominated by three-body *pnd* breakup (see Fig. 17).

However, despite the prediction that all high-$p_{miss}$ events will result in a three-body *pnd* final state, we expect that there will be a significant fraction of four-body *ppnn* final states, as well as three-body breakup followed by a *pd* rescattering, resulting in a four-body *ppnn* final state. These will not be fully reconstructable by the proposed measurement, since there are two undetected final state particles.

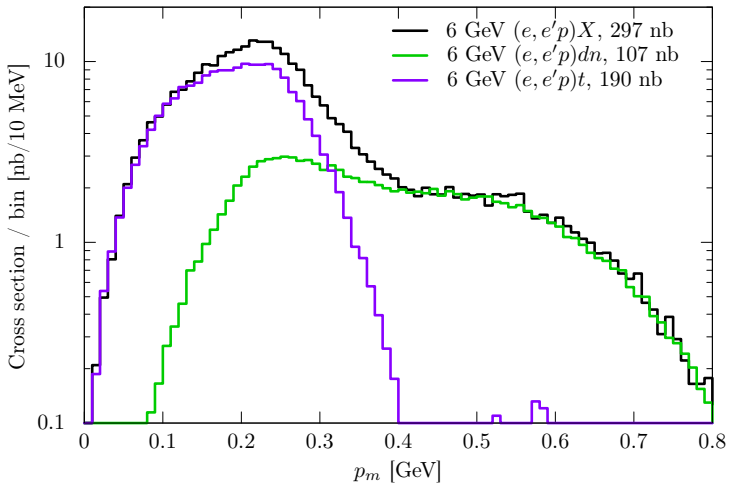


**FIG. 17:** Simulated cross section versus $p_{miss}$ for events passing the selection criteria for (black) all events, (purple) $(e,e'p)t$ events, and (green) $(e,e'p)dn$ events.

### *6. Deuteron Acceptance*

We simulated the acceptance of the spectator deuterons in ALERT in two steps: (1) A simulation of uniformly generated deuterons to determine the ALERT acceptance in momentum and angle and (2) a simulation of the expected deuteron momentum and angle distributions assuming spectator deuterons. We used the two simulations to determine the average deuteron acceptance probability in ALERT for the $^4$He$(e,e'pd_S)n$ reaction.

For the first step, we generated deuterons uniformly between 0 and 400 MeV/c momentum, 0 to 180° scattering angle and 0 to 360° in azimuthal angle. The events were passed through GEMC [59], the CLAS12 Geant4 based simulation framework, including the ALERT detector. We required at least eight hits in the drift chamber to accept a deuteron track. We assumed any track with hits in all 8 DC layers could be reconstructed; we did not do any track reconstruction.

Fig. 18 shows the acceptance for deuterons in momentum and scattering angle. Larger energy deposition means better signal to noise in the ALERT detector and hence a higher detection efficiency. We selected a conservative range in momentum and angle where the detection efficiency is expected to be larger than 90%. The limits are

$$100 < \ p_d \ < 300\,\mathrm{MeV/c}, \tag{8}$$

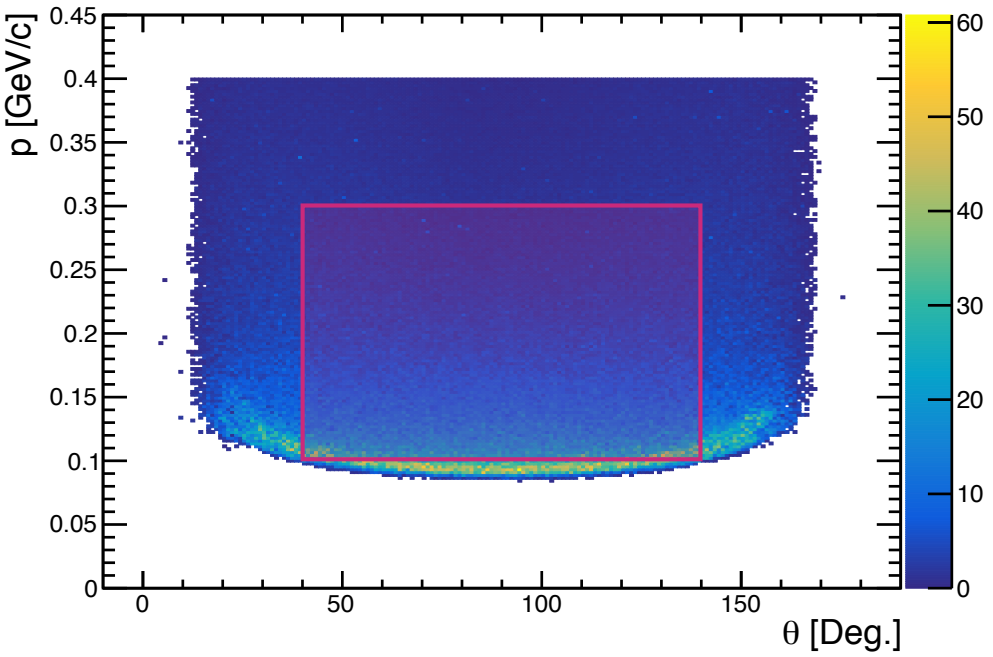


**FIG. 18:** Simulated deuteron acceptance in ALERT as a function of momentum and scattering angle. The colors indicate the total energy deposition of the deuteron in MeV in the ALERT detector. The purple box shows the range of deuteron momentum and angle used for the deuteron acceptance estimation.

$$40^\circ < \theta_d < 140^\circ. \tag{9}$$

These limits are indicated by the purple box in Fig. 18 and are similar to the limits for protons and $^4$He recoils shown in Fig. 3.10 in the initial ALERT proposal [51]. The estimated detection upper limit of 300 MeV/c is due to the decreased energy deposition in ALERT by the higher momentum deuterons.

For the second simulation, we assumed that deuterons would be emitted isotropically with momentum equal and opposite to that of the center of mass momentum $\vec{p}_{cm}$ of the $np$ SRC pair in $^4$He. $\vec{p}_{cm}$ was measured by [7] using $^4\mathrm{He}(e,e'pn)X$ in Hall A. They measured a Gaussian distribution for $\vec{p}_{cm}$ of the $pn$ pair with a width of $100 \pm 20$ MeV/c in each cartesian direction. This was also calculated to be about 84 MeV/c by Wiringa *et al.* using *ab inito* Quantum Monte Carlo calculations [60]. We randomly generated 100,000 deuterons

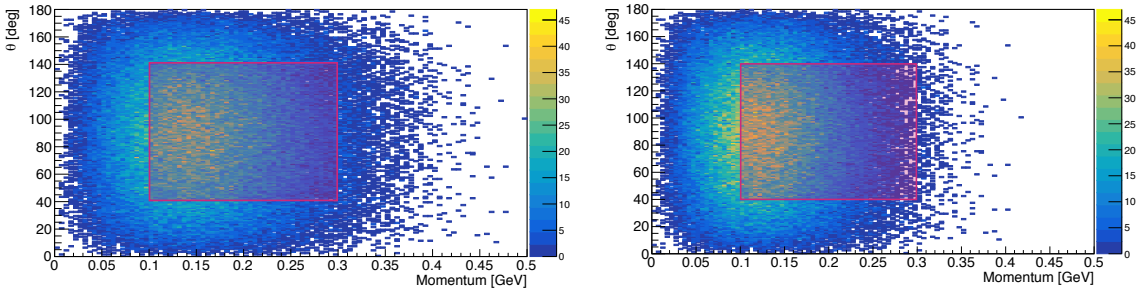


**FIG. 19:** Simulated deuteron total momentum versus scattering angle distribution if momentum is sampled from Gaussian with $\sigma = 100\,\mathrm{MeV/c}$ (left) and $\sigma = 84\,\mathrm{MeV/c}$ (right) in each momentum direction. The purple box shows the (conservative) ALERT deuteron momentum and angle acceptance.

following each of these distributions.

Fig. 19 shows the deuteron total momentum versus angle distribution for $\sigma(p_{cm}) = 100$ MeV/c (left) and $\sigma(p_{cm}) = 84$ MeV/c (right). The (conservative) ALERT acceptance is shown by the red box. This gives an ALERT deuteron acceptance of 59% for $\sigma(p_{cm}) = 100$ MeV/c. If $\sigma(p_{cm}) = 84$ MeV/c then the deuteron acceptance is 53%. We lowered this to 50% to include the finite ALERT detection efficiency. The upper detection limit of 300 MeV/c has only a small effect on the overall detection efficiency.

### 7. *Triton Acceptance*

We also checked the acceptance of ALERT for tritons. Similar to Sec. III B 6, we generated tritons uniformly between 0 and 400 MeV/c momentum, 0 to 180° in scattering angle, and 0 to 360° in azimuthal angle. The events were passed through GEMC [59] with the ALERT detector. We required at least eight hits in the drift chamber to accept a triton track. As for the deuteron acceptance, we assumed any track with hits in all eight DC layers could be reconstructed; we did not do any track reconstruction.

All tritons which passed the selection are shown in Fig. 20. It shows the acceptance for triton in momentum and scattering angle. Larger energy deposition means better signal to noise in the ALERT detector and hence a higher detection efficiency. We can see that ALERT will cover tritons from 120 to 300 MeV/c momentum.

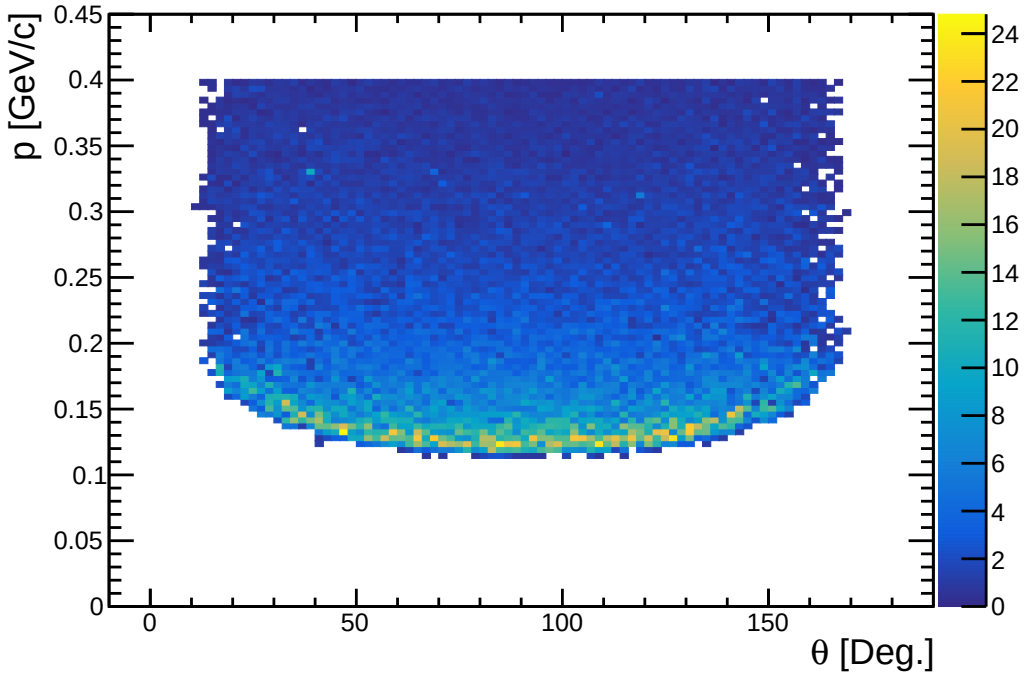


**FIG. 20:** Simulated triton energy acceptance in ALERT as a function of momentum and triton angle. The colors indicate the total energy deposition of the triton in the ALERT detector in MeV.

Since the triton momentum is equal to the missing momentum (see Fig. 17), this will allow us to measure the $^4$He$(e,e't_S)p$ reaction from $p_{miss}$ = 120 MeV/c up to at least 300 MeV/c, in order to measure the relative fractions of $pt$, $pnd$ and $ppnn$ final states.

### *8. Expected Number of Events and Beam Time*

We determined the expected number of high-$p_{miss}$ (e.g., SRC) $^4$He$(e,e'pd_S)n$ events from the number of RGM $^4$He$(e,e'p)$ SRC events. We then corrected this for several effects:

1. the deuteron acceptance of ALERT (0.5)
2. the deuteron survival probability (0.1)
3. $\phi$-gaps in ALERT and the contributions of $pp$ pairs to the RGM events (0.8)
4. FSI ($pn$ rescattering) events in the RGM data set removed by a cut on $\theta_{pn}$ (0.1)

resulting in:

$$N_{(e,e'pd_S)n} = N_{(e,e'p)^{RGMSRC}} f_{\text{accept}} f_{\text{emit}} f_{\phi gap} f_{FSI} \quad (10)$$

$$= (3.8 \times 10^5) \times 0.5 \times 0.1 \times 0.8 \times 0.1 \quad (11)$$

$$= 1.6 \times 10^3. \quad (12)$$

This gives a minimum expected number of events of $1.6 \times 10^3$. This will allow us to measure the $\vec{p}_{rel}$-$\vec{p}_{cm}$ correlation (see Fig. 2) and the transition from mean field to SRC (see Fig. 3). This corresponds to 16 PAC days at the ALERT luminosity.

We did not directly estimate the number of expected low $p_{miss}$ events (both $(e, e'pd_S)n$ and $(e, e't)p$), since it is expected to be far larger than the number of SRC events (see Fig. 17).

Fig. 21 shows the expected result for the $\vec{p}_{rel}$-$\vec{p}_{cm}$ correlation with 1600 events (left). It is based on the quasi-elastic simulations from Sec. III B 5, using the proton distribution from the spectral function, an isotropic deuteron distribution, and the conservative limits of the deuteron acceptance in ALERT (see Sec. III B 6). The resulting distribution is not flat due to the deuteron acceptance. The statistical precision is shown for 1600 events and 20 bins. This is almost two orders of magnitude better than what was observed at JINR experiment [48].

Fig. 22 shows a possible distribution of the opening angle between $\vec{p}_{miss}$ and $\vec{p}_n$ as a function of neutron momentum. We combined an isotropic mean-field distribution at $p_n \leq 0.22$ GeV/c with the SRC neutrons from Sec. III B 5. We smeared the reconstructed neutron momentum using the expected momentum resolution. We will use this plot (after deconvolution for the neutron momentum resolution) to determine the width of the SRC-meanfield transition region.

These two plots indicate that we need a minimum of 1600 events to determine the degree of correlation between $\vec{p}_{rel}$ and $\vec{p}_{cm}$ (and hence the validity of scale separation) and to measure the transition region from mean-field to SRC.

In summary, we request 16 PAC days at 6.4 GeV beam energy to collect at least 1600 $^4$He$(e, e'pd)n$ events in SRC dominant regions of phase space and far more than that in mean-field dominant regions. We request an additional PAC day to change beam energy, to commission the ALERT detector at 6.4 GeV and to optimize detector energy thresholds for deuteron detection over the full momentum range. Table I summarizes the request.

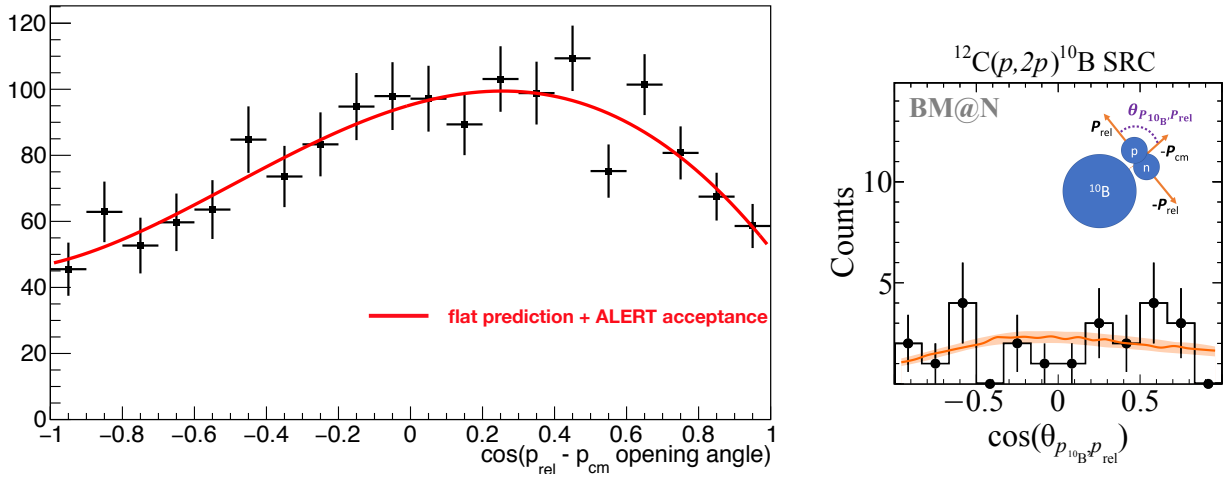


**FIG. 21:** Expected results: the number of counts plotted versus the opening angle between $\vec{p}_{rel}$ and $\vec{p}_{cm}$ for SRC events. Events were simulated with an isotropic uncorrelated $\vec{p}_{cm}$ and the resulting shape is due to the deuteron acceptance. (left) The expected results from 1600 $^4\mathrm{He}(e,e'pd)n$ events; (right) the previous results from $^{12}\mathrm{C}(p,2p^{10}B)n$ at JINR [48].

| **Configuration** | **Target** | **Luminosity** $\mathrm{cm}^{-2}\mathrm{s}^{-1}$ | **Beam current** nA | **Beam energy** GeV | **Beam time request** days |
|---|---|---|---|---|---|
| Measurement Days | $^4$He | $3 \cdot 10^{34}$ | 500 | 6.4 | 16 |
| Commissioning | $^4$He | various | various | 6.4 | 1 |
| **Total** | | | | | **17** |

**TABLE I:** Summary of requested beam time and beam parameters.

## IV. RELATION TO OTHER APPROVED EXPERIMENTS

The CLAS12 RGM experiment measured $^4$He at 6 GeV using the standard CLAS configuration. This lets them measure electrons and leading protons or neutrons in the forward detector, as well as the SRC-partner recoil protons and neutrons in the central detector with momenta $p_N \geq 350$ MeV/c. The CD cannot detect low momentum recoil nucleons or nuclei. In contrast, by detecting the spectator $d$ in the $^4\mathrm{He}(e,e'pd_S)n$ reaction, the proposed measurement will be able to reconstruct SRC-partner recoil neutrons over a far wider mo-

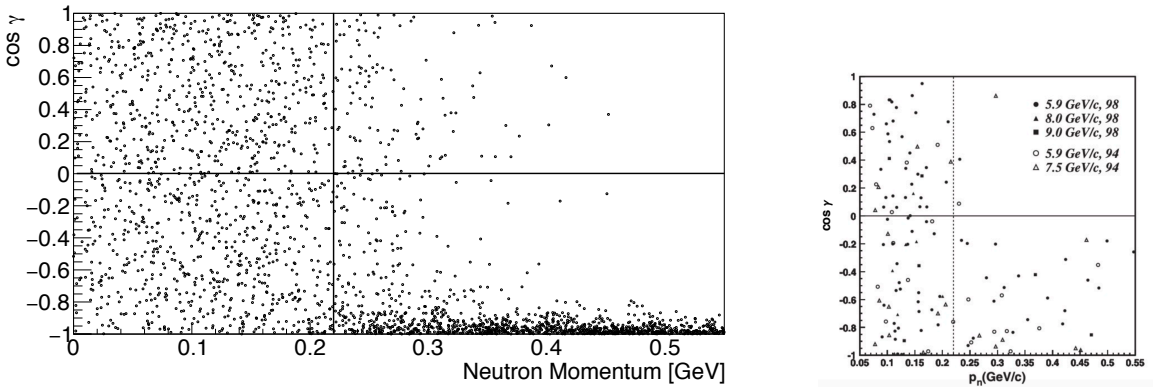


**FIG. 22:** Expected results: (left) $\cos\gamma$, the opening angle between the reconstructed neutron momentum $\vec{p}_n$ and the missing momentum $\vec{p}_{miss}$, showing the transition from mean field to SRC. The low-$p_n$ events, $p_n \leq 220$ MeV/c, are thrown isotropically, the higher $p_n$ events are thrown using the simulations from Sec. III B 5 and the conservative limits of the deuteron acceptance (see Sec. III B 6). The results include the expected reconstructed neutron momentum resolution of 80 MeV/c. The plot contains the expected 1600 of $(e, e'pd)n$ SRC events for the proposed measurement and an additional 1600 low-momentum (mean field) events. (right) the previous results for C$(p, 2pn)$ [9].

mentum range and determine the exact nuclear final state of the reaction. Both of these are critical to testing factorization through the independence of $\vec{p}_{cm}$ and $\vec{p}_{rel}$ and to measuring the transition from mean field to SRC degrees of freedom in the nucleus.

In contrast, RGM will focus on other aspects of SRCs, including the ratio $pn$ to $pp$ pairs, and measuring the relative momentum distribution over a wide range of nuclei.

[1] O. Hen, G. A. Miller, E. Piasetzky, and L. B. Weinstein, Rev. Mod. Phys. **89**, 045002 (2017), 1611.09748.

[2] C. Ciofi degli Atti, Phys. Rept. **590**, 1 (2015).

[3] J. Carlson, S. Gandolfi, F. Pederiva, S. C. Pieper, R. Schiavilla, K. E. Schmidt, and R. B. Wiringa, Rev. Mod. Phys. **87**, 1067 (2015), 1412.3081.

[4] J. Arrington, D. W. Higinbotham, G. Rosner, and M. Sargsian, Prog. Part. Nucl. Phys. **67**, 898 (2012), 1104.1196.

[5] L. Frankfurt, M. Sargsian, and M. Strikman, Int. J. Mod. Phys. **A23**, 2991 (2008), 0806.4412.

[6] O. Hen et al., Science **346**, 614 (2014), 1412.0138.

[7] I. Korover et al. (Lab Hall A), Phys. Rev. Lett. **113**, 022501 (2014), 1401.6138.

[8] R. Subedi et al., Science **320**, 1476 (2008), 0908.1514.

[9] E. Piasetzky, M. Sargsian, L. Frankfurt, M. Strikman, and J. W. Watson, Phys. Rev. Lett. **97**, 162504 (2006), nucl-th/0604012.

[10] N. Fomin et al., Phys. Rev. Lett. **108**, 092502 (2012), 1107.3583.

[11] K. S. Egiyan et al. (CLAS), Phys. Rev. Lett. **96**, 082501 (2006), nucl-ex/0508026.

[12] L. L. Frankfurt, M. I. Strikman, D. B. Day, and M. Sargsian, Phys. Rev. **C48**, 2451 (1993).

[13] L. B. Weinstein, E. Piasetzky, D. W. Higinbotham, J. Gomez, O. Hen, and R. Shneor, Phys. Rev. Lett. **106**, 052301 (2011), 1009.5666.

[14] O. Hen, E. Piasetzky, and L. B. Weinstein, Phys. Rev. **C85**, 047301 (2012), 1202.3452.

[15] O. Hen, D. W. Higinbotham, G. A. Miller, E. Piasetzky, and L. B. Weinstein, International Journal of Modern Physics E **22**, 1330017 (2013), https://www.worldscientific.com/doi/pdf/10.1142/S0218301313300178, URL https://www.worldscientific.com/doi/abs/10.1142/S0218301313300178.

[16] D. Higinbotham, G. A. Miller, O. Hen, and K. Rith, CERN Cour. **53N4**, 24 (2013), 1305.7143.

[17] O. Hen, A. Accardi, W. Melnitchouk, and E. Piasetzky, Phys. Rev. **D84**, 117501 (2011), 1110.2419.

[18] O. Hen, B.-A. Li, W.-J. Guo, L. B. Weinstein, and E. Piasetzky, Phys. Rev. **C91**, 025803 (2015), 1408.0772.

[19] B.-A. Li, B.-J. Cai, L.-W. Chen, and J. Xu, Prog. Part. Nucl. Phys. **99**, 29 (2018), 1801.01213.

[20] B.-A. Li, W.-J. Guo, and Z. Shi, Phys. Rev. **C91**, 044601 (2015), 1408.6415.

[21] G. A. Miller, A. Beck, S. May-Tal Beck, L. B. Weinstein, E. Piasetzky, and O. Hen (2018), 1805.12099.

[22] O. Hen, L. B. Weinstein, E. Piasetzky, G. A. Miller, M. M. Sargsian, and Y. Sagi, Phys. Rev. **C92**, 045205 (2015), 1407.8175.

[23] M. M. Sargsian, Phys. Rev. **C89**, 034305 (2014), 1210.3280.

[24] M. Martini, M. Ericson, and G. Chanfray, Phys. Rev. **D85**, 093012 (2012), 1202.4745.

[25] H. Gallagher, G. Garvey, and G. P. Zeller, Ann. Rev. Nucl. Part. Sci. **61**, 355 (2011).

[26] R. Weiss, R. Cruz-Torres, N. Barnea, E. Piasetzky, and O. Hen, Phys. Lett. **B780**, 211 (2018), 1612.00923.

[27] R. Cruz-Torres, A. Schmidt, G. A. Miller, L. B. Weinstein, N. Barnea, R. Weiss, E. Piasetzky, and O. Hen, Phys. Lett. B **785**, 304 (2018), 1710.07966.

[28] F. Simkovic, A. Faessler, H. Muther, V. Rodin, and M. Stauf, Phys. Rev. **C79**, 055501 (2009), 0902.0331.

[29] R. Weiss, A. W. Denniston, J. R. Pybus, O. Hen, E. Piasetzky, A. Schmidt, L. B. Weinstein, and N. Barnea, Phys. Rev. C **103**, L031301 (2021), 2005.01621.

[30] R. Cruz-Torres, D. Lonardoni, R. Weiss, N. Barnea, D. W. Higinbotham, E. Piasetzky, A. Schmidt, L. B. Weinstein, R. B. Wiringa, and O. Hen, Nature Phys. **17**, 306 (2021), 1907.03658.

[31] C. Colle, O. Hen, W. Cosyn, I. Korover, E. Piasetzky, J. Ryckebusch, and L. B. Weinstein, Phys. Rev. **C92**, 024604 (2015), 1503.06050.

[32] W. Cosyn and J. Ryckebusch, Phys. Lett. B **820**, 136526 (2021), 2106.01249.

[33] J. Ryckebusch, W. Cosyn, S. Stevens, C. Casert, and J. Nys, Phys. Lett. B **792**, 21 (2019), 1808.09859.

[34] D. Lonardoni, S. Gandolfi, X. B. Wang, and J. Carlson (2018), 1804.08027.

[35] S. N. More, S. K. Bogner, and R. J. Furnstahl, Phys. Rev. **C96**, 054004 (2017), 1708.03315.

[36] O. Hen et al. (CLAS), Phys. Lett. **B722**, 63 (2013), 1212.5343.

[37] M. Duer et al. (CLAS), Submitted (2017).

[38] H. Baghdasaryan et al. (CLAS), Phys. Rev. Lett. **105**, 222501 (2010), 1008.3100.

[39] A. Tang et al., Phys. Rev. Lett. **90**, 042301 (2003), nucl-ex/0206003.

[40] R. Shneor et al. (Jefferson Lab Hall A), Phys. Rev. Lett. **99**, 072501 (2007), nucl-ex/0703023.

[41] M. Duer et al. (CLAS), under internal review (2018).

[42] R. Schiavilla, R. B. Wiringa, S. C. Pieper, and J. Carlson, Phys. Rev. Lett. **98**, 132501 (2007), nucl-th/0611037.

[43] M. M. Sargsian, T. V. Abrahamyan, M. I. Strikman, and L. L. Frankfurt, Phys. Rev. **C71**, 044615 (2005), nucl-th/0501018.

[44] M. Alvioli, C. Ciofi degli Atti, and H. Morita, Phys. Rev. Lett. **100**, 162503 (2008).

[45] M. Alvioli, C. Ciofi degli Atti, and H. Morita, Phys. Rev. **C94**, 044309 (2016), 1607.04103.

[46] M. Alvioli, C. Ciofi degli Atti, L. P. Kaptari, C. B. Mezzetti, H. Morita, and S. Scopetta, Phys. Rev. **C85**, 021001 (2012), 1112.2651.

[47] C. Ciofi degli Atti and S. Simula, Phys. Rev. **C53**, 1689 (1996), nucl-th/9507024.

[48] M. Patsyuk et al., Nature Phys. **17**, 693 (2021), 2102.02626.

[49] I. Korover et al. (CLAS) (2022), 2209.01492.

[50] V. D. Burkert et al., Nucl. Instrum. Meth. A **959**, 163419 (2020).

[51] W. Armstrong et al., *Partonic Structure of Light Nuclei* (2017), nucl-ex/1708.00888.

[52] E. O. Cohen, O. Hen, E. Piasetzky, L. B. Weinstein, M. Duer, A. Schmidt, I. Korover, and H. Hakobyan (CLAS) (2018), 1805.01981.

[53] A. Schmidt et al. (CLAS), Nature **578**, 540 (2020), 2004.11221.

[54] B. Schmookler et al. (CLAS), Nature **566**, 354 (2019), 2004.12065.

[55] I. Korover et al. (CLAS), Phys. Lett. B **820**, 136523 (2021), 2004.07304.

[56] T. De Forest, Nucl. Phys. A **392**, 232 (1983).

[57] Z. Ye, J. Arrington, R. J. Hill, and G. Lee, Phys. Lett. B **777**, 8 (2018), 1707.09063.

[58] Rocco, N. and Lovato, A., In preparation.

[59] https://gemc.jlab.org/gemc/html/index.html.

[60] R. B. Wiringa, R. Schiavilla, S. C. Pieper, and J. Carlson, Phys. Rev. C **89**, 024305 (2014), URL https://link.aps.org/doi/10.1103/PhysRevC.89.024305.